Conferment of CO-controlled Dimer–Monomer Transition Property to Thermostable Cytochrome *c*' by Mutation in the Subunit–Subunit Interface

Masaru Yamanaka,[1] Ryoko Nakayama,[1] Sotaro Fujii,[2] Satoshi Wakai,[3] Yoshihiro Sambongi,[2] and Shun Hirota*[1]

[1]Division of Materials Science, Graduate School of Science and Technology, Nara Institute of Science and Technology, 8916-5 Takayama-cho, Ikoma, Nara 630-0192, Japan

[2]Graduate School of Biosphere Science, Hiroshima University, 1-4-4 Kagamiyama, Higashi-Hiroshima, Hiroshima 739-8528, Japan

[3]Graduate School of Science, Technology and Innovation, Kobe University, 1-1 Rokkodai-cho, Nada-ku, Kobe, Hyogo 657-8501, Japan

E-mail: hirota@ms.naist.jp

Masaru Yamanaka received his Ph.D. in agriculture from Hiroshima University in 2012. Following postdoctoral work at Hiroshima University with Prof. Yoshihiro Sambongi (2010) and Okazaki Institute for Integrative Bioscience with Prof. Shigetoshi Aono (2010-2012), he joined the Graduate School of Materials Science (reorganized to Graduate School of Science and Technology in 2018) at Nara Institute of Science and Technology as an assistant professor in 2012. His current research interests are protein engineering by utilizing oligomeric sensor proteins.

Shun Hirota received his Ph.D. from the Graduate University for Advanced Studies in 1995 under the supervision of Prof. Teizo Kitagawa. After he was a JSPS research fellow and postdoctoral researcher in the Institute of Molecular Science at the Okazaki National Research Institutes and in the Department of Chemistry at Emory University, he joined Nagoya University as an Assistant Professor in 1996, and became an Associate Professor at Kyoto Pharmaceutical University in 2002. He was invited as a Full Professor to Nara Institute of Science and Technology in April 2007. His research interests include structures, functions, and reaction mechanisms of metalloproteins.

Abstract

Cytochrome *c*' (CP) is a gas-binding homo-dimeric heme protein. Mesophilic *Allochromatium vinosum* CP (AVCP) and thermophilic *Hydrogenophilus thermoluteolus* CP (PHCP) have high sequence and structure similarities. AVCP is known to exhibit a dimer–monomer transition upon CO binding/dissociation, whereas detailed CO-binding properties of PHCP remain unrevealed. Here, we found that the CO-binding affinity of wild-type PHCP is lower than that of AVCP, and the PHCP dimer does not dissociate to monomers under CO-saturated reduced conditions. The CO-binding affinity of PHCP increased by mutations in the subunit–subunit interface (F11T, T18F, or F71D). The T18F, F71D, and T18F/F71D PHCP variants exhibited similar dimer–monomer transitions upon CO binding/dissociation to that of AVCP, although the F11T variant did not. The simulated structures of the PHCP variants revealed that the T18F and F71D mutations caused rearrangement in the subunit–subunit interface, whereas the F11T mutation did not, indicating that the effective dimer–monomer transitions upon CO binding/dissociation are induced by the rearrangement in the subunit–subunit interface. The present results indicate that subunit–subunit interface mutation of oligomeric proteins is a useful approach in the adjustment of protein stability and ligand binding affinity, leading to a change in the quaternary structural property.

Keywords: Dimer–monomer transition, Gas-binding, Subunit–subunit interface

1. Introduction

Many proteins undergo structural changes by ligand binding in cells, where the structural changes are frequently related to their functions,[1-4] such as signal transduction and gene expression.[5-7] The heme, protoporphyrin IX iron complex, is an important prosthetic group in proteins for ligand binding. It functions as gas-binding centers for O_2, NO, and CO, in sensor proteins.[8-11] Cytochrome *c*' (CP), which belongs to the Ambler's class II cytochrome *c* family, has been found in various Gram-negative bacteria.[12,13] The physiological role of CP is presumed to be NO binding involved in the cellular response to NO.[14-21] CP typically forms a homo-dimer with a four-helix bundle subunit, and each subunit possesses a covalently bound five-coordinate heme for gas-binding.[21-23] A conserved His residue is coordinated axially to the heme iron in CPs, whereas Leu, Met, Phe, or Tyr is located at the sixth coordination site of the heme iron without a coordination bond.[21,24-29]

Allochromatium vinosum CP (AVCP) forms a homo-dimeric structure in the oxidized and reduced states, and exhibits a unique dimer–monomer transition upon ligand binding/dissociation.[30-32] In AVCP, the sixth heme coordination site, which is a possible ligand binding site, is occupied with the side chain of Tyr16 without a coordination bond. Tyr16 has been suggested to function as a trigger for the dimer–monomer transition in AVCP upon ligand binding/dissociation, where changes in the subunit–subunit interaction are induced by the conformational change of the Tyr16 side chain through the ligand binding to the heme iron.[31]

Thermophilic *Hydrogenophilus thermoluteolus* CP (PHCP; the same bacterium was previously named *Pseudomonas hydrogenothermophila*) exhibits a high similarity with AVCP in amino acid sequence and three-dimensional structure; 55% amino acid sequence identity, homo-dimeric structure with four-helix bundle subunits and Tyr16 at the heme

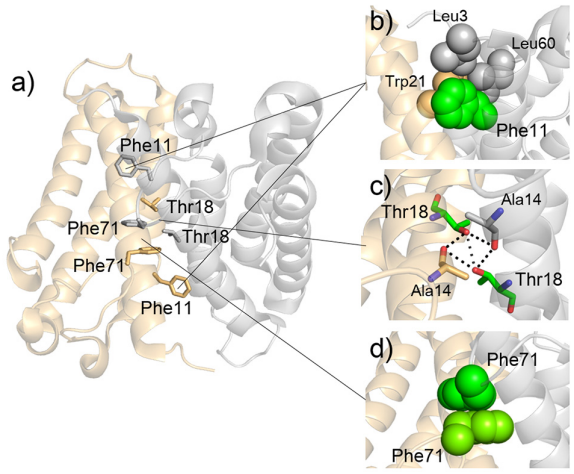

Figure 1. X-ray crystal structure of wild-type PHCP (PDB: 5B3I). The light orange and gray regions in the dimer correspond to each subunit. Phe11, Thr18, and Phe71 are labeled with residue numbers. a) The overall structure of PHCP dimer. The side chains of Phe11, Thr18, and Phe71 are shown as stick models. b) The hydrophobic interactions around Phe11. The side chain atoms of Leu3, Phe11, Trp21, and Leu60 are shown as sphere models. Phe11 is highlighted in green. c) Hydrogen bonding network comprising Ala14 and Thr18 of both subunits. The atoms of Ala14 and Thr18 are shown as stick models. The hydrogen bonds (< 3.2 Å) are depicted in broken lines. Thr18 is highlighted in green. The nitrogen and oxygen atoms are depicted in blue and red, respectively. d) π–π stacking between the two Phe71 residues of the respective subunits. The side chain atoms of Phe71 are shown as sphere models. Phe71 is highlighted in green.

sixth coordination site.[33,34] PHCP also binds exogenous ligands such as CO and NO, although PHCP is more stable than AVCP.[34] Three of the six residues responsible for the high stability of PHCP are located in the subunit–subunit interface: Phe11, Thr18, and Phe71 (Figure 1).[34] Phe11 forms a hydrophobic packing with Leu3 and Leu60 of the same subunit and Trp21 of the other subunit. The two Thr18(Oγ1) and two Ala14(O) residues of the respective subunits form an inter-subunit hydrogen-bonding network at the center of the subunit–subunit interface. The two Phe71 residues of the respective subunits π–π stack with each other.

A deeper understanding of the relation between protein stability and conformational change will be useful for the future design of functional oligomeric proteins. However, the CO-binding affinity and the effect of CO-binding on the quaternary structure of PHCP have not been revealed. In this study, we investigated the CO-binding properties of PHCP in detail, in terms of CO-binding affinity and the quaternary structural change upon CO binding/dissociation. The CO-binding affinity of wild-type PHCP was lower than that of AVCP, and the PHCP dimer did not dissociate to monomers under CO-saturated reduced conditions, although Tyr16 occupies the sixth position of the heme proximal site as in AVCP. However, the T18F and F71D PHCP variants, which possess the corresponding amino acids of AVCP in the subunit–subunit interface, exhibited the dimer-to-monomer transition upon CO binding.

2. Experimental

Preparation of Wild-type PHCP and Variants. Wild-type PHCP and its variant plasmids were prepared as reported previously.[34] Phe11, Thr18, and Phe71 in the subunit–subunit interface were substituted to Thr (F11T), Phe (T18F), and Asp (F71D), respectively, which are the corresponding residues of AVCP. The T18F/F71D double and F11T/T18F/F71D triple variants were prepared by multistep mutagenesis using plasmids and primers of the single variants.[34]

The expressions of recombinant wild-type PHCP and its variants were performed as reported previously.[35] *E. coli* JCB387 cells containing plasmid pKK223-3 (encoding PHCP) and plasmid pEC86 (encoding cytochrome *c* maturation proteins) were grown in LB broth for 22 h at 37 °C. The cells were harvested by centrifugation, and suspended in 50 mM potassium phosphate buffer, pH 7.0, containing 5 mM potassium ferricyanide. After sonication, the cell lysate was centrifuged to remove cell debris. The supernatant was purified with ammonium sulfate; the impurities were removed as a precipitate with 40% ammonium sulfate, and subsequently PHCP was collected as a precipitate with 70% ammonium sulfate. The precipitate was dissolved in 50 mM potassium phosphate buffer, pH 7.0, and dialyzed against 25 mM sodium acetate buffer, pH 5.0. The dialyzed solution was centrifuged, and the obtained supernatant was purified by a HiTrap SP cation exchange column (GE Healthcare, IL, USA) with the same buffer at 4 °C. PHCP was eluted with a 0–300 mM NaCl gradient using a fast protein liquid chromatography (FPLC) system (Biologic DuoFlow 10, Bio-rad, CA, USA). Subsequently, PHCP was purified with a HiLoad 26/600 Superdex 75 pg gel filtration column (GE Healthcare) using the FPLC system with 50 mM potassium phosphate buffer, pH 7.0, at 4 °C. The PHCP fraction was collected and further purified with a mono Q anion exchange column (GE Healthcare) using the FPLC system with 20 mM Tris-HCl buffer, pH 8.0, and a 0−300 mM NaCl gradient at 4 °C. The molecular mass of PHCP was confirmed by MALDI-TOF mass spectrometry (Autoflex II, Bruker, MA, USA) using sinapinic acid as a matrix. The concentrations of the proteins were calculated from the absorbances of the Soret bands using the absorption coefficients of the oxidized forms (399 nm for wild-type, F11T, T18F, F71D, and T18F/F71D PHCP; 402 nm for F11T/T18F/F71D PHCP) obtained by the pyridine hemochrome method:[36] wild-type PHCP, 9.1×10^4 $M^{-1}cm^{-1}$; F11T, 9.5×10^4 $M^{-1}cm^{-1}$; T18F, 9.6×10^4 $M^{-1}cm^{-1}$; F71D, 9.3×10^4 $M^{-1}cm^{-1}$; T18F/F71D, 9.2×10^4 $M^{-1}cm^{-1}$; F11T/T18F/F71D, 10.2×10^4 $M^{-1}cm^{-1}$.

Optical Absorption and Circular Dichroism Measurements. UV-vis spectra of wild-type PHCP and its variants (heme unit, 5 μM) in the oxidized and reduced states in 50 mM potassium phosphate buffer, pH 7.0, were obtained with a UV-2450 spectrophotometer (Shimadzu, Kyoto, Japan) using a 1-cm-pathlength quartz cell at 25 °C. Reduced PHCP was obtained by an addition of sodium dithionite (final concentration, 2 mM) under a N_2 atmosphere using a vacuum line. Binding of CO to reduced PHCP was achieved by incubation of the reduced protein solution at 25 °C under a CO atmosphere.

Circular dichroism (CD) spectra of oxidized wild-type PHCP and its variants (heme unit, 10 μM) in 50 mM potassium phosphate buffer, pH 7.0, were obtained with a J-725 spectrometer (Jasco, Tokyo, Japan) using a 0.1-cm-pathlength quartz cell at 25 °C.

CO-binding Affinity Measurements. The reduced states of wild-type PHCP and its variants (heme unit, 8 μM) were obtained as described above. The CO association constants (K_a) of PHCP were calculated from the CO

concentration-dependent increase in the 418 nm absorbance, which corresponds to the Soret band of the CO-bound form. A CO-saturated buffer was prepared by introducing CO to a buffer solution using the vacuum line, and was added to the protein solution to attain desired CO concentrations (0–500 μM). The CO concentration of the sample solution was calculated using the CO concentration of CO-saturated water: 27.6 mg/L (985 μM) at 25 °C.[37] The protein concentration was normalized taking into account the dilution of the protein solution by the addition of CO-saturated buffer.

Size Exclusion Chromatography Analysis. The quaternary structural changes of wild-type PHCP and its variants upon CO binding/dissociation were analyzed by size exclusion chromatography (SEC). The solution containing PHCP (heme unit, 20 μM) was analyzed with a Superdex 75 10/300 GL gel filtration column (GE Healthcare) using the Biologic DuoFlow 10 FPLC system (Bio-rad) with the following conditions; flow rate, 0.5 mL/min; monitoring wavelength, 399, 418, and 426 nm, corresponding to the Soret band wavelengths of the oxidized, CO-bound, and reduced forms, respectively; solvent, 50 mM potassium phosphate buffer, pH 7.0; temperature, 4 °C. The reduced and CO-bound forms of PHCP were analyzed with the same conditions as those for the oxidized forms, except for the solvent of 50 mM potassium phosphate buffer, pH 7.0, containing 5 mM sodium dithionite and saturated with N_2 and CO, respectively.

Thermal Denaturation Analysis. The thermal stability of the T18F/F71D PHCP double variant (heme unit, 20 μM) in 20 mM potassium phosphate, pH 7.0, was evaluated by monitoring the CD ellipticity at 222 nm with a J-820 CD spectrometer (Jasco) using a 0.1-cm-pathlength quartz cell.[35,38,39] The CD ellipticity was measured from 25 to 150 °C with 0.5 °C intervals by increasing the temperature at a rate of 1.0 °C/min. The reversibility of protein denaturation was examined as described previously.[34,35]

The CD ellipticity was plotted against the temperature, and the data were subjected to nonlinear least squares fitting with a two-state unfolding model as described previously.[40] The data were corrected using the slopes of the baselines for the native and denatured forms, and normalized to calculate the fraction of denatured proteins. The fraction of denatured proteins was plotted as a function of temperature, and the midpoint temperature for protein denaturation (T_m) was obtained. The enthalpy change (ΔH) during protein denaturation at T_m was obtained by the analysis with the van't Hoff equation.[38,41] The entropy change upon protein denaturation of wild-type PHCP (ΔS_{wt}) was calculated from the equation, $\Delta S_{wt} = \Delta H / T_m$. The differences between wild-type PHCP and its variants in the free energy change by denaturation were calculated using ΔS_{wt} and the equation given by Becktel and Schellman,[42] $\Delta\Delta G_m = \Delta T_m \times \Delta S_{wt}$, where ΔT_m represents the difference in T_m between wild-type PHCP and a variant.

Structural Simulation Analysis. Three-dimensional model structures of the oxidized F11T, T18F, F71D, and T18F/F71D PHCP variants were simulated by energy minimization of the crystal structure of oxidized wild-type PHCP (PDB: 5B3I) with residue substitution using molecular mechanics with a MOE calculation system (Chemical Computing Group Inc., Quebec, Canada). The structures of wild-type PHCP and its variants were compared using the molecular graphic program, PyMOL.[43]

3. Results and Discussion

Optical Absorption and CD Spectra of Wild-type PHCP and Variants. The Soret bands of wild-type PHCP in the oxidized and reduced forms and the reduced form under a CO-saturated condition were observed at 399, 426, and 418 nm, respectively, similar to the wavelengths reported previously (Figure 2).[34] The Soret band wavelengths of the PHCP variants

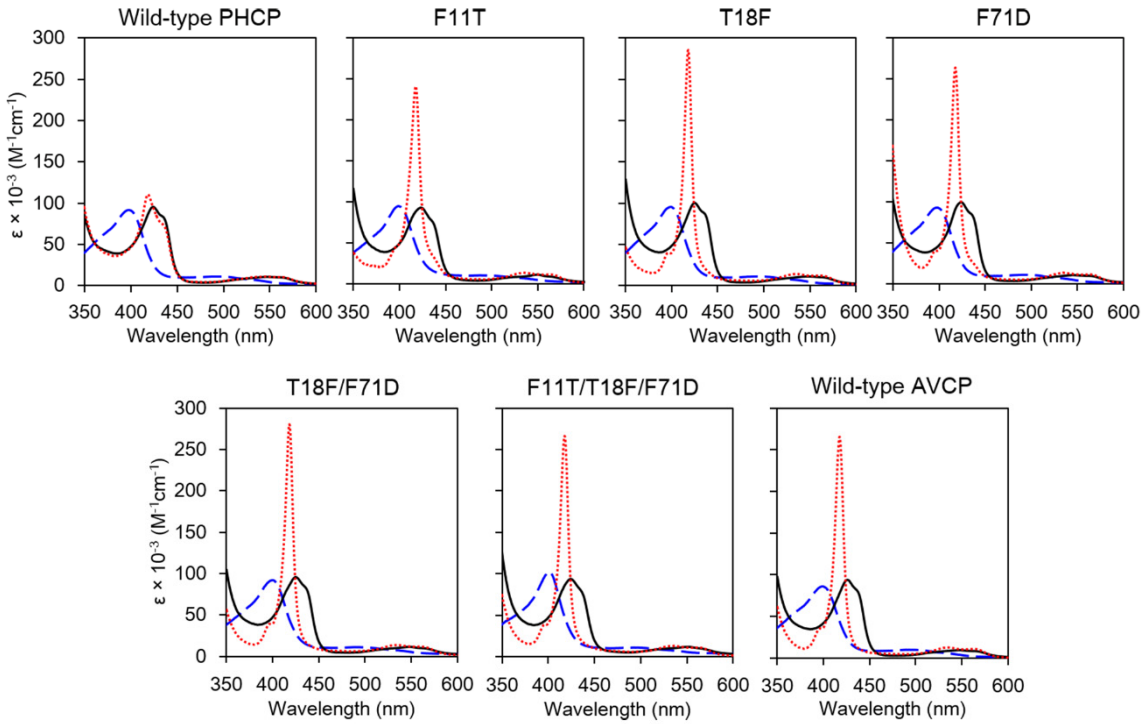

Figure 2. Absorption spectra of oxidized and reduced wild-type PHCP, its variants, and wild-type AVCP. The oxidized forms were measured under air (blue broken line), and the reduced forms were measured under N_2 (black solid line) and CO atmospheres (red dotted line). Measurement conditions: sample concentration (heme unit), 8 μM; solvent, 50 mM potassium phosphate buffer; pH, 7.0; temperature, 25 °C.

in the oxidized forms were similar to that of oxidized wild-type PHCP, except for that of the F11T/T18F/F71D triple variant observed at 402 nm. The Soret band wavelengths of the PHCP variants in the reduced forms under N_2 atmospheres were all similar to that of reduced wild-type PHCP. The Soret bands of reduced wild-type PHCP and its PHCP variants blue-shifted to 418 nm by exchanging the atmospheres from N_2 to CO. The Soret band intensity of the wild-type PHCP spectrum obtained under CO-saturated reduced conditions was lower than that of CO-bound AVCP (Figure 2), indicating a lower CO-binding affinity of wild-type PHCP compared to that of AVCP. However, the intensities of the Soret bands of reduced PHCP variants increased significantly by exchanging the atmospheres from N_2 to CO, where the intensity increases were similar to that of AVCP under similar conditions (Figure 2), suggesting similar CO-binding properties for the PHCP variants as AVCP.

The CD spectra of oxidized PHCP variants in potassium phosphate buffer, pH 7.0, at 25 °C exhibited negative peaks at 208 and 222 nm, similar to the spectrum of oxidized wild-type PHCP (Figure S1). These results indicate that the secondary α-helical structures of the variants was not changed significantly from those of wild-type PHCP.

CO-binding Affinities of Wild-type PHCP and Variants. The K_a values of wild-type PHCP, its variants, and AVCP for CO binding were obtained by measuring the absorbance at the Soret band wavelength (418 nm) of the CO-bound form under various CO concentrations (Figure S2). The K_a values of wild-type PHCP and AVCP for CO binding were obtained as 9.4×10^2 and 6.8×10^4 M^{-1}, respectively (Table 1). The K_a value of wild-type PHCP was significantly lower than the AVCP K_a value, which was in good agreement with the value reported previously (7.0×10^4 M^{-1}).[44] The K_a values of CO binding were obtained as 1.9×10^3, 4.8×10^3, 3.2×10^3, 3.2×10^5, and 2.1×10^5 M^{-1} for the F11T, T18F, F71D, T18F/F71D, and F11T/T18F/F71D PHCP variants, respectively, where the K_a values of the PHCP variants were all higher than that of wild-type PHCP (Table 1). Mutations of three residues (F11T, T18F, and F71D) in the PHCP subunit–subunit interface responsible for the protein stability enhanced the CO-binding affinity (Table 1 and Figure S2), indicating that these residues are related to not only the protein stability but also the ligand binding property. The T18F/F71D and F11T/T18F/F71D multiple variants exhibited K_a values 200–300 times higher than that of wild-type PHCP, whereas the K_a values of the single variants were only 2–5 times higher than that of the wild-type protein. These results reveal that multiple mutations are more effective than single mutations for PHCP on increasing the CO-binding affinity.

Table 1. CO-binding affinities of wild-type PHCP, its variants, and wild-type AVCP.

Protein	Affinity [M^{-1}][a)]	
wild-type PHCP	9.4×10^2	(1.2×10^2)
F11T PHCP	1.9×10^3	(3.3×10^2)
T18F PHCP	4.8×10^3	(6.5×10^2)
F71D PHCP	3.2×10^3	(7.3×10^2)
T18F/F71D PHCP	3.2×10^5	(9.0×10^3)
F11T/T18F/F71D PHCP	2.1×10^5	(2.5×10^4)
wild-type AVCP	6.8×10^4	(5.5×10^3)

[a)]The values are shown in averages (standard deviations) of three independent experiments.

Quaternary Structural Change upon CO Binding/Dissociation. SEC analysis was performed to investigate the quaternary structural changes of wild-type PHCP and its variants upon CO binding/dissociation (Figure 3). An elution peak which corresponded to a dimer was detected around 11 mL in the SEC chromatograms of oxidized and reduced wild-type PHCP (Figures 3 and S3). The elution peak at ~11 mL of oxidized and reduced wild-type PHCP did not shift under CO-saturated reduced conditions, while the elution peak of oxidized AVCP at ~11 mL shifted to 12–13 mL under CO-saturated reduced conditions.[45] These results indicate that the wild-type PHCP dimer does not dissociate to monomers under CO-saturated reduced conditions that AVCP dissociates.

All PHCP variants used in this study exhibited elution peaks at ~11 mL in the oxidized and reduced forms, suggesting that these variants maintain the dimeric structures in the oxidized and reduced forms as wild-type PHCP (Figures 3 and S3). However, the F11T variant did not exhibit a clear peak shift in the SEC chromatogram under CO-saturated reduced conditions. Under CO-saturated reduced conditions, T18F, F71D, T18F/F71D and F11T/T18F/F71D variants exhibited peak shifts in the SEC chromatograms to larger elution volumes at 12–13 mL. These elution volumes corresponded to 2/3–1/2 molecular sizes of the dimer, indicating that the T18F and F71D mutations allow PHCP to suffer dimer–monomer transition upon CO binding, where the extent of the peak shift in the SEC chromatogram of each variant depends on its

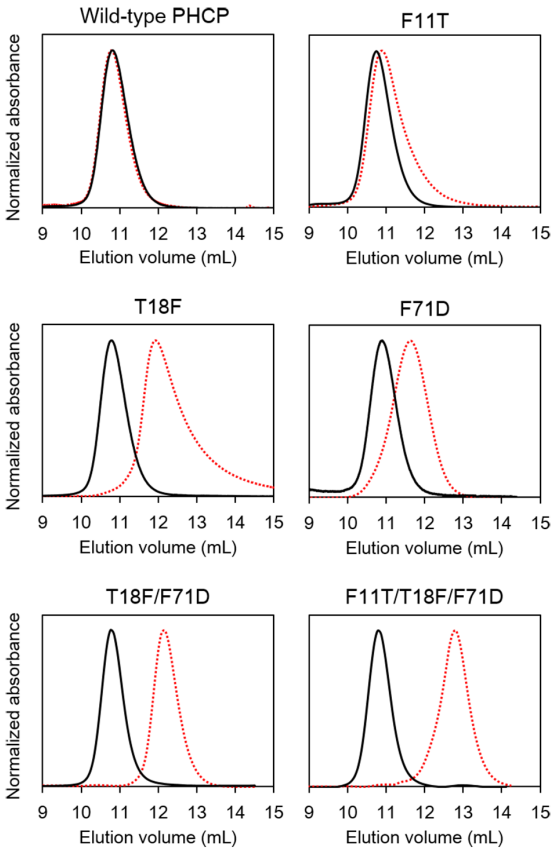

Figure 3. Size exclusion chromatograms of wild-type PHCP and its variants. Elution curves of PHCP in the oxidized forms under air (black solid lines) and the reduced forms under CO-saturated conditions (red dotted lines) are depicted. Measurement conditions: initial protein concentration (heme unit), 20 μM; column, Superdex 75 10/300 GL; flow rate, 0.5 ml/min; monitoring wavelength, 399 and 418 nm for oxidized and CO forms, respectively; solvent, 50 mM potassium phosphate buffer; pH 7.0; temperature, 4 °C. The elution curves are normalized according to the maximum intensity.

dimer–monomer equilibrium. By re-oxidation of the CO-bound reduced PHCP variants with potassium ferricyanide and removal of CO from the heme iron, the SEC elution curves exhibited peaks at ~11 mL (Figure S4). These results demonstrate that the dimer–monomer transitions of the PHCP variants with T18F and/or F71D mutations are reversible upon CO binding/dissociation, similar to the dimer–monomer transition of AVCP upon CO binding/dissociation.

The CO-binding affinity of PHCP was two-orders lower than that of AVCP (K_m; PHCP, 9.4×10^2 M^{-1}; AVCP, 6.8×10^4 M^{-1}), and PHCP did not exhibit a quaternary structural change under CO-saturated reduced conditions (Figure 3). Interestingly, the effect on CO-binding affinity for each mutation in PHCP was similar, but the effect on the quaternary structural change upon CO binding varied (i.e., the T18F and F71D mutations clearly displayed dimer–monomer transitions upon CO binding/dissociation, but the F11T mutation did not).

Thermal Stabilities of PHCP Variants. The thermal stability of the oxidized T18F/F71D double variant was measured by means of the CD ellipticity change during thermal denaturation (Figure 4), whereas the thermal stabilities of F11T, T18F, F71D, and F11T/T18F/F71D PHCP variants have been measured previously.[34] The T_m value of the T18F/F71D variant was estimated as 74.0 ± 0.2 °C, which was similar to that of the F11T/T18F/F71D triple variant (74.3 ± 0.4 °C).[34] The difference in the denaturation free energy changes ($\Delta\Delta G_m$) between the T18F/F71D double variant and wild-type PHCP was estimated as -28.5 ± 0.4 kJ/mol, which was similar to that between the F11T/T18F/F71D triple variant and wild-type PHCP (-28.1 ± 0.8 kJ/mol),[34] indicating that the T18F/F71D variant was destabilized to a similar extent as that of the F11T/T18F/F71D variant.

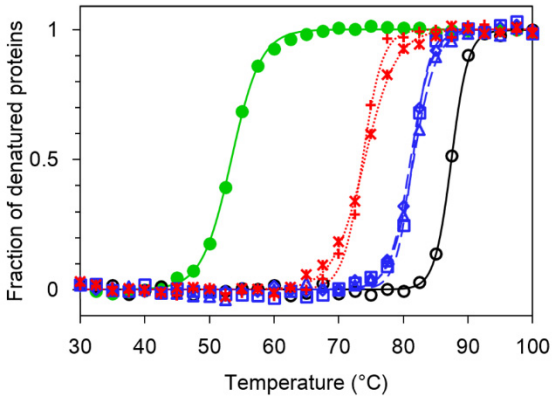

Figure 4. Thermal denaturation curves of oxidized wild-type PHCP, its variants, and wild-type AVCP. The thermal denaturation curve of the T18F/F71D PHCP variant obtained in the present study is depicted together with the thermal denaturation curves of wild-type PHCP, its other variants (F11T, T18F, F71D, and F11T/T18F/F71D), and wild-type AVCP obtained in previous studies,[34,35] The fraction of denatured proteins is plotted as a function of temperature with the least-square fitted curve of a two-state unfolding model. The data are depicted in different colors and symbols; wild-type PHCP (black solid line and open circles), its single variants (blue broken lines; open symbols of triangles, squares, and diamonds for F11T, T18F, and F71D, respectively) and multiple variants (red dotted lines; crosses and asterisks for T18F/F71D and F11T/T18F/F71D, respectively), and wild-type AVCP (green solid line and closed circles). Measurement conditions: sample concentration (heme unit), 20 μM; solvent, 20 mM potassium phosphate buffer; pH, 7.0; temperature, 25–150 °C; temperature increasing rate, 1.0 °C/min; monitoring wavelength, 222 nm.

The quaternary structural change upon ligand binding/dissociation is a useful property for biomaterials, such as molecular sensors and ligand controllable molecular switches. Recently, AVCP oligomers, which reversibly dissociate to dimers upon CO binding/dissociation, have been constructed by utilizing domain-swapped dimers.[45] In addition to a high CO affinity and a dimer–monomer transition property upon CO binding/dissociation for the T18F/F71D PHCP variant (Table 1 and Figure 3), its stability was higher than that of AVCP (T_m: T18F/F71D PHCP, 74.0 °C; AVCP, 52.4 °C) (Figure 4). These properties may be advantageous for construction of gas sensors and gas-controllable molecules.

Structural Simulation of PHCP Variants. Structural simulations based on energy calculations were performed for the PHCP variants to obtain structural insights into the dimer–monomer transition upon CO binding/dissociation. The crystal structure of wild-type PHCP (PDB: 5B3I) was used as a template to perform energy minimization calculation by molecular mechanics.[34] The hydrophobic packing between Thr11, Leu3, and Leu60 of one subunit and Trp21 of the other subunit was retained in the simulated structure of the F11T variant (Figure 5a). In the T18F variant, the Thr18 substitution to Phe caused the loss of the inter-subunit hydrogen bonding network comprising Thr18(Oγ1) and Ala14(O) of the two subunits. A water molecule bound to the wild-type protein was pushed out from the inter-subunit space by the bulky side chain of the substituted Phe18 in the T18F variant; thus, the inter-subunit hydrogen bonding network observed in wild-type PHCP among Thr18(O) and Asn22(Nδ2) of one subunit, Ser15(Oγ) and Ser55(Oγ) of the other subunit, and the bound water at the inter-subunit space was not detected in the T18F variant (Figure 5b). For the F71D variant, π–π stacking between the two Phe71 residues in the subunit–subunit interface was removed, and the subunit–subunit interface was partially exposed to the solvent (Figure 5c). Each structural change observed in the simulated structure of the T18F and F71D variant at the subunit–subunit interface compared to the wild-type PHCP structure was reproduced in the simulated structure of the T18F/F71D double variant. However, there was no significant change in the size of the gas-binding channel from the solvent to the sixth coordination site of the heme iron, as well as the distance between the Tyr16 side chain and the heme iron, in the simulated structures of PHCP variants compared to that of wild-type PHCP.

No structural evidence for the enhancement of CO-binding affinity in the PHCP variants was detected in their simulated structures. The well-packed subunit–subunit interface in wild-type PHCP may prevent the conformational change of the Tyr16 side chain and thus inhibit CO to bind to the heme iron, as a result lowering the CO-binding affinity. However, the PHCP variants were less stable compared to wild-type PHCP (Figure 4). The substitutions of F11T, T18F, and F71D in PHCP may partially loosen the packing of the residues at the subunit–subunit interface, making Tyr16 feasible to change its side chain conformation upon CO binding and, as a result, enhancing the CO-binding affinity.

The hydrogen bonding network including Thr18 and π–π stacking of Phe71 at the subunit–subunit interface of PHCP are more important than the hydrophobic interaction around Phe11 for the stabilization of the dimer (Figure 1), although Phe11, Thr18, and Phe71 exhibited similar effects on the thermostability of PHCP (Figure 4). Phe11 may inhibit the conformational change of Tyr16 upon CO binding to the heme

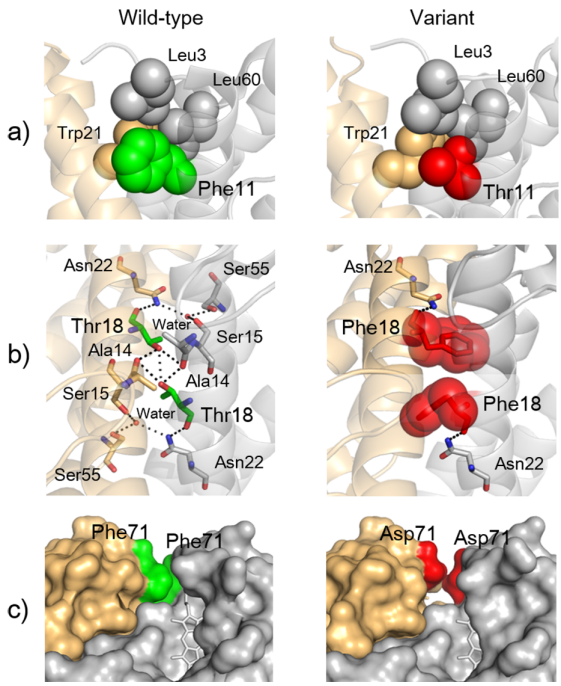

Figure 5. Structure comparisons between oxidized wild-type PHCP and its variants. The crystal structure of wild-type PHCP (PDB: 5B3I) is shown in the left side, and simulated structures of PHCP variants are shown in the right side. The light orange and gray regions in the dimer correspond to each subunit. a) Structure comparison between wild-type PHCP and the F11T variant. The side chain atoms of the residues contributing to hydrophobic interactions are shown as sphere models with residue numbers. Phe11 is highlighted in green in the wild-type protein, and Thr11 is highlighted in red in the F11T variant. b) Structure comparison between wild-type PHCP and the T18F variant. The atoms of the residues forming a hydrogen bonding network are shown as stick models with residue numbers. The hydrogen bonds (< 3.2 Å) are depicted in broken lines. The nitrogen and oxygen atoms are depicted in blue and red, respectively. The side chain of Phe18 in the T18F variant is shown as sphere models with transparency. Thr18 is highlighted in green in the wild-type protein, and Phe18 is highlighted in red in the T18F variant. c) Structure comparison between wild-type PHCP and the F71D variant. The surface structures of the proteins are shown. Phe71 of the wild-type protein is highlighted in green, and Asp71 of the F71D variant is highlighted in red. The hemes are shown as stick models.

iron, owing to the hydrophobic interactions around Phe11. For the F11T variant, the hydrophobic interactions around Phe11 were perturbed, allowing Tyr16 to change its conformation, although the subunit–subunit interface interactions by Thr18 and Phe71 were strong enough to inhibit the dimer dissociation even when Tyr16 changes its conformation. The structural rearrangements by the T18F and F71D mutations in PHCP may destabilize the dimer by loosening the interaction between the subunits. The structural change of the Tyr16 side chain initiated by CO binding to the heme may effectively expand to other residues in the subunit–subunit interface in the variants, resulting in dissociation of the dimer to monomers in a similar mechanism as that proposed for the dimer dissociation of AVCP.[31] It has been proposed through structural comparison between AVCP and other CPs that the Tyr16 side chain of AVCP is pushed out from the heme pocket when CO binds to the heme iron, and the conformational change of the Tyr16 side chain initiates flips in the heme propionate and Glu17 side chain (Figure S5).[46] The flipped Glu17 side chain suffers steric hindrance with other residues, causing the dimer to dissociate to monomers. However, the side chain of Thr17 (corresponding to Glu17 in AVCP) in PHCP is shorter than that of Glu17 in AVCP; and accordingly, the steric hindrance of Thr17 with the residues of the other subunit in PHCP may be reduced compared to that of Glu17 in AVCP (Figure S5). Thus, the steric hindrance between the flipped Glu17 and the residues of the other subunit may not be essential for the dimer-to-monomer dissociation in the PHCP variants. For a further understanding of the molecular mechanism of the dimer–monomer transition upon CO binding/dissociation of PHCP, detailed analyses, such as the X-ray crystal structure of CO-bound monomeric PHCP subunit, are necessary.

4. Conclusion

Wild-type thermophilic PHCP exhibited a lower CO-binding affinity compared to that of mesophilic AVCP, and did not exhibit a dimer–monomer transition under CO-saturated reduced conditions. The CO-binding affinity of PHCP was increased by substitution of the subunit–subunit interface residues—responsible for the high protein stability—to the corresponding residues in AVCP. Distinct dimer–monomer transitions upon CO binding/dissociation were observed for the PHCP variants with T18F and/or F71D mutations, and these mutations induced CO-dependent quaternary structural changes. The present results demonstrate that modifications in the stability and quaternary structural feature of oligomeric proteins are achievable by mutations of key residues in the subunit–subunit interface.

We thank Mr. Leigh McDowell, Nara Institute of Science and Technology, for his advice on manuscript preparation. This work was partially supported by Grants-in-Aid for Scientific Research (Category C, Grant No. JP18K04906 to M.Y.; Category B, Grant No. JP18H02088 to S.H.) from JSPS.

Supporting Information

Figures S1–S5 are available as Supporting Information. This material is available on http://dx.doi.org/10.1246/bcsj.xxxxx

References

1. M. Gerstein, A. M. Lesk, C. Chothia, *Biochemistry* **1994**, *33*, 6739.
2. S. Hammes-Schiffer, S. J. Benkovic, *Annu. Rev. Biochem.* **2006**, *75*, 519.
3. C. J. Tsai, A. Del Sol, R. Nussinov, *Mol. Biosyst.* **2009**, *5*, 207.
4. E. Ahmad, G. Rabbani, N. Zaidi, M. A. Khan, A. Qadeer, M. Ishtikhar, S. Singh, R. H. Khan, *J. Biomol. Struct. Dyn.* **2013**, *31*, 630.
5. M. Lewis, *C. R. Biol.* **2005**, *328*, 521.
6. D. M. Rosenbaum, S. G. F. Rasmussen, B. K. Kobilka, *Nature* **2009**, *459*, 356.
7. H. Sawai, M. Yamanaka, H. Sugimoto, Y. Shiro, S. Aono, *J. Biol. Chem.* **2012**, *287*, 30755.
8. M. A. Gilles-Gonzalez, G. Gonzalez, *J. Inorg. Biochem.* **2005**, *99*, 1.
9. T. A. K. Freitas, J. A. Saito, S. Hou, M. Alam, *J. Inorg. Biochem.* **2005**, *99*, 23.
10. S. Aono, *Dalton trans.* **2008**, 3137.
11. H. M. Girvan, A. W. Munro, *J. Biol. Chem.* **2013**, *288*, 13194.
12. M. D. Kamen, L. P. Vernon, *J. Bacteriol.* **1954**, *67*, 617.

13. R. P. Ambler, *Biochim. Biophys. Acta* **1991**, *1058*, 42.
14. T. Yoshimura, H. Iwasaki, S. Shidara, S. Suzuki, A. Nakahara, T. Matsubara, *J. Biochem.* **1988**, *103*, 1016.
15. T. Yoshimura, S. Shidara, T. Ozaki, H. Kamada, *Arch. Microbiol.* **1993**, *160*, 498.
16. T. Yoshimura, S. Fujii, H. Kamada, K. Yamaguchi, S. Suzuki, S. Shidara, S. Takakuwa, *Biochim. Biophys. Acta* **1996**, *1292*, 39.
17. N. J. Watmough, G. Butland, M. R. Cheesman, J. W. B. Moir, D. J. Richardson, S. Spiro, *Biochim. Biophys. Acta* **1999**, *1411*, 456.
18. R. Cross, J. Aish, S. J. Paston, R. K. Poole, J. W. B. Moir, *J. Bacteriol.* **2000**, *182*, 1442.
19. R. Cross, D. Lloyd, R. K. Poole, J. W. B. Moir, *J. Bacteriol.* **2001**, *183*, 3050.
20. P. S. Choi, V. M. Grigoryants, H. D. Abruña, C. P. Scholes, J. P. Shapleigh, *J. Bacteriol.* **2005**, *187*, 4077.
21. M. A. Hough, C. R. Andrew, *Adv. Microb. Physiol.* **2015**, *67*, 1.
22. M. A. Cusanovich, Q. H. Gibson, *J. Biol. Chem.* **1973**, *248*, 822.
23. G. R. Moore, *Biochim. Biophys. Acta* **1991**, *1058*, 38.
24. B. C. Finzel, P. C. Weber, K. D. Hardman, F. R. Salemme, *J. Mol. Biol.* **1985**, *186*, 627.
25. A. J. Dobbs, B. F. Anderson, H. R. Faber, E. N. Baker, *Acta Crystallogr. D Biol. Crystallogr.* **1996**, *52*, 356.
26. S. Benini, W. R. Rypniewski, K. S. Wilson, S. Ciurli, *J. Inorg. Biochem.* **2008**, *102*, 1322.
27. Y. Hirano, Y. Kimura, H. Suzuki, K. Miki, Z. Y. Wang, *Biochemistry* **2012**, *51*, 6556.
28. D. Kekilli, F. S. Dworkowski, G. Pompidor, M. R. Fuchs, C. R. Andrew, S. Antonyuk, R. W. Strange, R. R. Eady, S. S. Hasnain, M. A. Hough, *Acta Crystallogr. D Biol. Crystallogr.* **2014**, *70*, 1289.
29. A. Manole, D. Kekilli, D. A. Svistunenko, M. T. Wilson, P. S. Dobbin, M. A. Hough, *J. Biol. Inorg. Chem.* **2015**, *20*, 675.
30. M. L. Doyle, S. J. Gill, M. A. Cusanovich, *Biochemistry* **1986**, *25*, 2509.
31. Z. Ren, T. Meyer, D. E. McRee, *J. Mol. Biol.* **1993**, *234*, 433.
32. T. H. Evers, J. L. van Dongen, E. W. Meijer, M. Merkx, *J. Biol. Inorg. Chem.* **2007**, *12*, 919.
33. S. Fujii, M. Masanari, M. Yamanaka, S. Wakai, Y. Sambongi, *Biosci. Biotechnol. Biochem.* **2014**, *78*, 1191.
34. S. Fujii, H. Oki, K. Kawahara, D. Yamane, M. Yamanaka, T. Maruno, Y. Kobayashi, M. Masanari, S. Wakai, H. Nishihara, T. Ohkubo, Y. Sambongi, *Protein Sci.* **2017**, *26*, 737.
35. S. Fujii, M. Masanari, H. Inoue, M. Yamanaka, S. Wakai, H. Nishihara, Y. Sambongi, *Biosci. Biotechnol. Biochem.* **2013**, *77*, 1677.
36. E. A. Berry, B. L. Trumpower, *Anal. Biochem.* **1987**, *161*, 1.
37. E. L. Pulster, J. V. Hillman, in *Hamilton and Hardy's Industrial Toxicology 6th edit*, ed. by R. D. Harbison, M. M. Bourgeois, G. T. Johnson, John Wiley & Sons, Inc., Hoboken, NJ, USA, **2015**, pp. 310.
38. A. Ohshima, S. Uchiyama, H. Nakano, T. Yoshida, T. Ohkubo, Y. Kobayashi, *Int. J. Pept. Res. Ther.* **2003**, *10*, 539.
39. M. Yamanaka, M. Masanari, Y. Sambongi, *Biochemistry* **2011**, *50*, 2313.
40. S. Uchiyama, A. Ohshima, S. Nakamura, J. Hasegawa, N. Terui, S.-i. J. Takayama, Y. Yamamoto, Y. Sambongi, Y. Kobayashi, *J. Am. Chem. Soc.* **2004**, *126*, 14684.
41. L. A. Marky, K. J. Breslauer, *Biopolymers* **1987**, *26*, 1601.
42. W. J. Becktel, J. A. Schellman, *Biopolymers* **1987**, *26*, 1859.
43. W. L. DeLano, *Drug Discov. Today* **2005**, *10*, 213.
44. A. L. Mayburd, R. J. Kassner, *Biochemistry* **2002**, *41*, 11582.
45. M. Yamanaka, M. Hoshizumi, S. Nagao, R. Nakayama, N. Shibata, Y. Higuchi, S. Hirota, *Protein Sci.* **2017**, *26*, 464.
46. T. H. Tahirov, S. Misaki, T. E. Meyer, M. A. Cusanovich, Y. Higuchi, N. Yasuoka, *Nat. Struct. Biol.* **1996**, *3*, 459.

Conferment of CO-controlled Dimer–Monomer Transition Property to Thermostable Cytochrome *c*' by Mutation in the Subunit–Subunit Interface

Masaru Yamanaka,[1] Ryoko Nakayama,[1] Sotaro Fujii,[2] Satoshi Wakai,[3] Yoshihiro Sambongi,[2] and Shun Hirota*[1]

[1]Division of Materials Science, Graduate School of Science and Technology, Nara Institute of Science and Technology, 8916-5 Takayama-cho, Ikoma, Nara 630-0192, Japan

[2]Graduate School of Biosphere Science, Hiroshima University, 1-4-4 Kagamiyama, Higashi-Hiroshima, Hiroshima 739-8528, Japan

[3]Graduate School of Science, Technology and Innovation, Kobe University, 1-1 Rokkodai-cho, Nada-ku, Kobe, Hyogo 657-8501, Japan

Contents

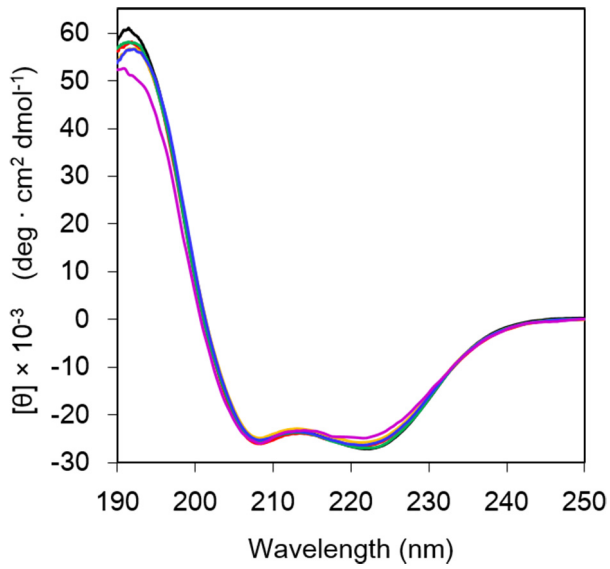

Figure S1. Far-UV circular dichroism spectra of oxidized wild-type PHCP and its variants: wild-type (black), F11T (red), T18F (orange), F71D (green), T18F/F71D (blue), and F11T/T18F/F71D (purple). Measurement conditions: sample concentration (heme unit), 10 μM; solvent, 50 mM potassium phosphate buffer; pH, 7.0; temperature, 25 °C.

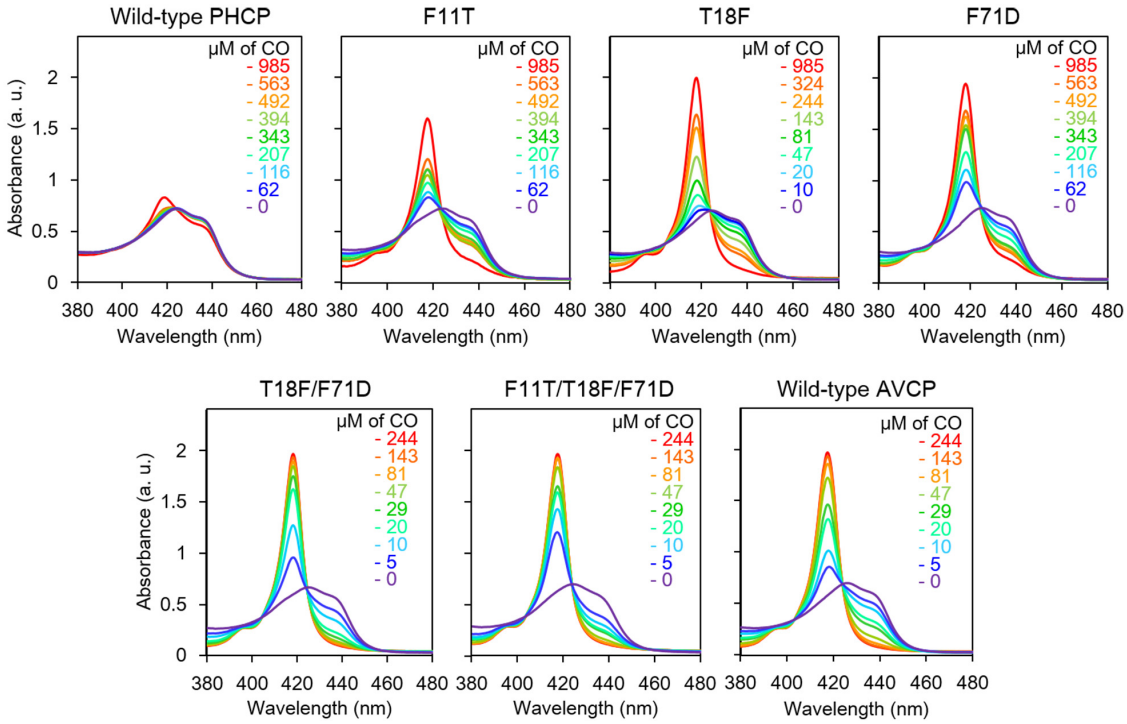

Figure S2. Absorption spectra of reduced wild-type PHCP, its variants, and wild-type AVCP under various CO concentrations. The CO concentrations are depicted in different colors as indicated in each figure. Measurement conditions: initial protein concentration (heme unit), 8 μM; solvent, 50 mM potassium phosphate buffer; pH, 7.0; temperature, 25 °C.

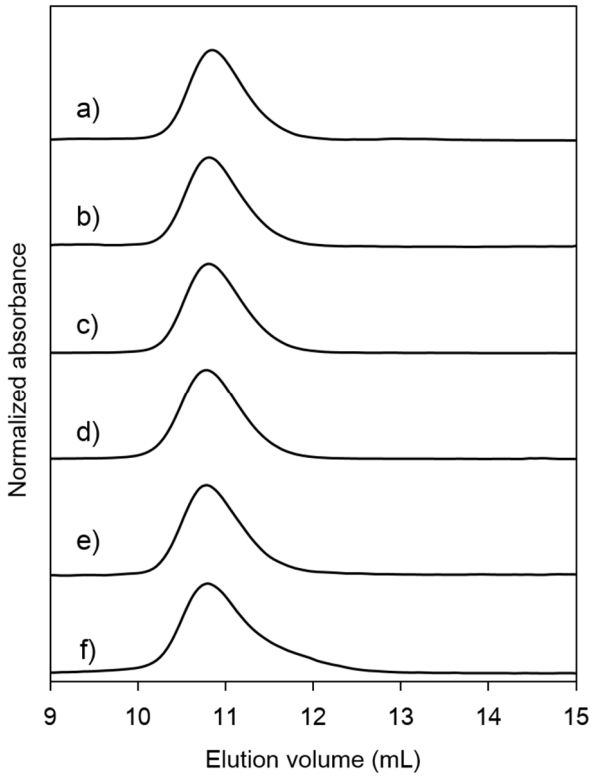

Figure S3. Size exclusion chromatograms of reduced wild-type PHCP and its variants. Elution curves of PHCP under N_2-saturated reduced conditions are depicted: (a) wild-type PHCP, and (b) F11T, (c) T18F, (d) F71D, (e) T18F/F71D, and (f) F11T/T18F/F71D variants. Measurement conditions: initial protein concentration (heme unit), 20 μM; column, Superdex 75 10/300 GL; flow rate, 0.5 ml/min; monitoring wavelength, 426 nm; solvent, 50 mM potassium phosphate buffer containing 5 mM sodium dithionite; pH 7.0; temperature, 4 °C. The elution curves are normalized according to the maximum intensity.

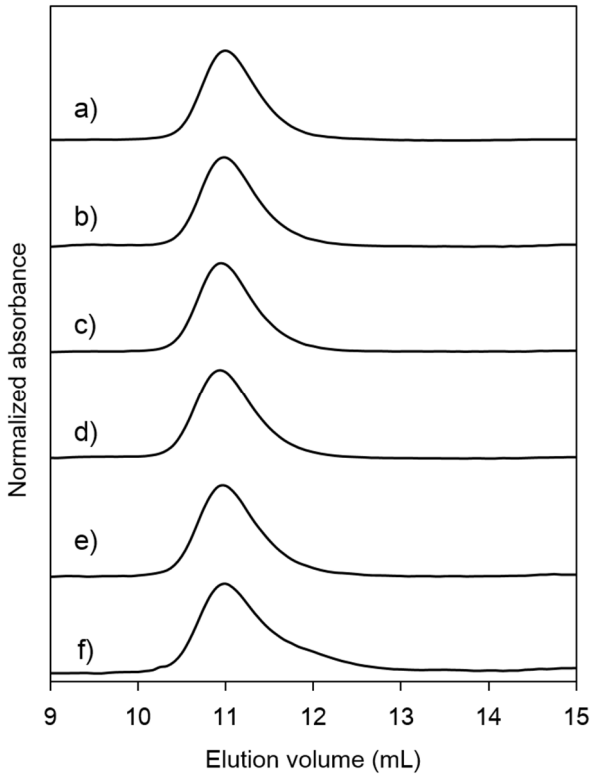

Figure S4. Size exclusion chromatograms of re-oxidized wild-type PHCP and its variants. Elution curves of the re-oxidized PHCP are depicted: (a) wild-type PHCP, and (b) F11T, (c) T18F, (d) F71D, (e) T18F/F71D, and (f) F11T/T18F/F71D variants. Measurement conditions: initial protein concentration (heme unit), 20 μM; column, Superdex 75 10/300 GL; flow rate, 0.5 ml/min; monitoring wavelength, 399 nm; solvent, 50 mM potassium phosphate buffer; pH 7.0; temperature, 4 °C. The elution curves are normalized according to the maximum intensity.

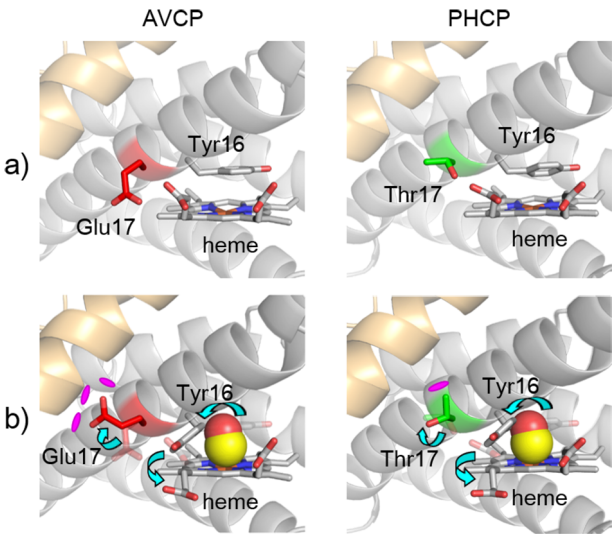

Figure S5. Structure comparisons between AVCP and PHCP. The structure of AVCP is shown in the left side, and that of PHCP is shown in the right side. The light orange and gray regions in the dimer correspond to each subunit. a) The crystal structures of wild-type AVCP (PDB: 1BBH) and wild-type PHCP (PDB: 5B3I). b) The assumed changes in the protein structures by CO binding to the heme iron. The CO-bound CP structures were obtained by changing the conformations of the Tyr16 side chain, Glu17 (AVCP) or Thr17 (PHCP) side chain, and heme propionate using PyMOL. The atoms of the side chains of Tyr16, Glu17, and Thr17 are shown as stick models with residue numbers. The hemes are also shown as stick models. The side chain of Glu17 is highlighted in red in AVCP, and that of Thr17 is highlighted in green in PHCP. The movements of residues and heme propionate by CO binding to the heme iron are indicated with arrows. The CO molecules are shown as sphere models (yellow and red), and the inter-subunit steric hindrances are depicted in magenta disks.